RSC Advances

PAPER

View Article Online
View Journal | View Issue

Cite this: *RSC Adv.*, 2017, **7**, 36015

NiO and Co_3O_4 co-doped g-C_3N_4 nanocomposites with excellent photoelectrochemical properties under visible light for detection of tetrabromobisphenol-A

Yi Liu,[a] Jizhou Jiang,[*ab] Yanjuan Sun,[a] Shengli Wu,[a] Yuan Cao,[a] Wanyun Gong[a] and Jing Zou[*a]

Received 29th April 2017
Accepted 14th July 2017

DOI: 10.1039/c7ra04822j

rsc.li/rsc-advances

Novel NiO/Co_3O_4/g-C_3N_4 nanocomposites with applications in photoelectrochemical sensing were designed and fabricated for the first time in this work. The morphology and microstructure of NiO/Co_3O_4/g-C_3N_4 were comprehensive investigated. The NiO/Co_3O_4/g-C_3N_4 nanocomposites exhibited higher photocurrent and donor density than those of pure g-C_3N_4, resulting in a higher photoelectrochemical activity for sensitive detection of TBBP-A in real water samples.

Tetrabromobisphenol-A (TBBP-A) is a brominated flame retardant and a persistent organic pollutant. It is widely used in many applications and has caused serious environmental problems and is a great threat to the ecological environment and human health because of its persistence, bioaccumulation and toxicity.[1–3] TBBP-A has been mainly detected in air,[4,5] water,[6,7] sewage sludge,[8,9] biological matrices[10,11] and soil.[12,13] Therefore, it is very important to monitor TBBP-A in organisms and environmental media rapidly and sensitively to assess the human and environmental risks of TBBP-A. Currently, several methods have been used to detect TBBP-A, such as gas chromatography-mass spectrometry (GC-MS), liquid chromatography-mass spectrometry (LC-MS), and tandem mass spectrometry (MS-MS).[14–16] Although these methods are effective in detecting TBBP-A accurately, they required large amounts of organic solvent and complicated pretreatment procedures.

In recent years, the photoelectrochemical sensing method, which offers a fast response, low cost and high sensitivity, is an emerging technique for the environmental and biological detection of analytes. Therefore, many high activity photoelectrochemical nanomaterials have been widely investigated. g-C_3N_4-based nanocomposite, which is a newly developed novel photoelectron nanocomposite, can be used as an electron mediator for effective separation of photo-generated electron–hole pairs at the junction interface.[17] Meanwhile, g-C_3N_4-based nanocomposites have also exhibited significantly improved optical and electrical activities,[18–20] making it one of the most promising materials for the photoelectrochemical sensing method. Therefore, many researchers have made significant efforts to improve the photoelectrochemical activity of g-C_3N_4 by coupling it with other semiconductors, metals or carbon materials. For example, Cai and co-workers[21] demonstrated a photoelectrochemical methodology for ultrasensitive detection of dopamine based on graphene/g-C_3N_4/TiO_2 nanocomposites, which showed a 0.02 μmol L^{-1} detection limit under the optimized conditions. Our group has also provided an improved method to sensing octylphenol with NiO and Ni co-doped g-C_3N_4. Our g-C_3N_4-based nanocomposites modified electrode showed high electrochemical activity to octylphenol under infrared light irradiation.[22] Another useful technique for quantitative assaying of T4 polynucleotide kinase activity based on Au/g-C_3N_4 nanohybrid was reported by Zhuang.[23] An 2D ternary nano-junction g-C_3N_4/N-graphene/MoS_2 was successfully designed and prepared, exhibiting an enhanced photoelectrochemical performance for simultaneous oxidation of methyl orange and reduction of Cr(VI).[24] Ag modified g-C_3N_4 film electrodes, which displayed a high photoelectrocatalytic activity for the degradation of methylene blue, were successfully prepared by a liquid-based reaction onto the ITO substrates.[25] The successful pairing of photoelectrochemical nanomaterials with a suitable doped catalyst is extremely important because the photoelectrochemical activity may be enhanced by improving the optical absorbance and separating photo-generated carriers at the junction interface. NiO and Co_3O_4 co-doped catalyst is probably one of the most ideal candidates due to their extraordinary inherent catalytic activity. Up to now, there have been no reports on detection of TBBP-A in real water samples by using photoelectrochemical technique with NiO and Co_3O_4 semiconductors co-doped g-C_3N_4 nanocomposites.

[a]*School of Chemistry and Environmental Engineering, School of Environmental Ecology and Bioengineering, Key Laboratory for Green Chemical Process of Ministry of Education, Wuhan Institute of Technology, Wuhan 430205, P. R. China. E-mail: jingzou@wit.edu.cn; 027wit@163.com*

[b]*Department of Physics, National University of Singapore, Singapore 117542. E-mail: phyjian@nus.edu.sg*

In this communication, NiO/Co_3O_4 co-doped g-C_3N_4 nanocomposites were successfully prepared by a step pyrolysis method, which is simple and low cost-effective. Nafion film electrodes were fabricated by dropping the mixture solution onto the glassy carbon electrode (GCE). The photoelectrochemical response of the g-C_3N_4/Nafion electrode significantly increased after modifying NiO/Co_3O_4 co-doped g-C_3N_4. On the basis of the NiO/Co_3O_4/g-C_3N_4 nanocomposites with excellent photoelectrochemical property, a simple and effective photoelectrochemical sensing method with a 0.1 μmol L^{-1} detection limit for sensitive detection of TBBP-A was developed through differential pulse voltammetry (DPV) under visible light irradiation. The photoelectrochemical sensing method was used for the analysis of TBBP-A in the real samples, and the precision and selectivity of the method were satisfactory.

NiO/Co_3O_4/g-C_3N_4 nanocomposites were prepared by pyrolysis method with a small amount of $NiCl_2 \cdot 6H_2O$ and $Co(NO_3)_3 \cdot 6H_2O$ mixtures and 3 g melamine heated at 500 °C for 4 h in a muffle furnace under air atmosphere. The modified electrode of NiO/Co_3O_4/g-C_3N_4/GCE was fabricated by dropping the NiO/Co_3O_4/g-C_3N_4 nanocomposites suspension on the surface of bare GCE and dried naturally.

The morphology and structure of the NiO/Co_3O_4/g-C_3N_4 nanocomposites and g-C_3N_4 sheets were characterized by TEM. Fig. 1b shows a typically sheet structure of g-C_3N_4. As shown in Fig. 1a, it can be seen that the NiO and Co_3O_4 nanoparticles with about 30 nm diameter were dispersed on the ultrathin g-C_3N_4 sheets. Meanwhile, the high resolution TEM (HR-TEM) image (Fig. 1c) reveals the interface between NiO and Co_3O_4 nanoparticles. The *d*-spacing values of 0.209 and 0.243 nm are clearly observed, which consist of the (200) plane of NiO and (311) plane of Co_3O_4, respectively. The clear lattice fringes indicate the high crystallinity of the nanocomposites, suggesting the successful preparation of NiO and Co_3O_4 co-doped g-C_3N_4 nanocomposites.

The crystalline structure of NiO/Co_3O_4/g-C_3N_4 nanocomposites and g-C_3N_4 sheets were characterized by XRD. In the XRD pattern of g-C_3N_4, the (002) peak at $2\theta = 27.4°$ reflected the characteristic interlayer stacking structure, while the (100) diffraction at 13.1° indicated the interplanar structural packing,

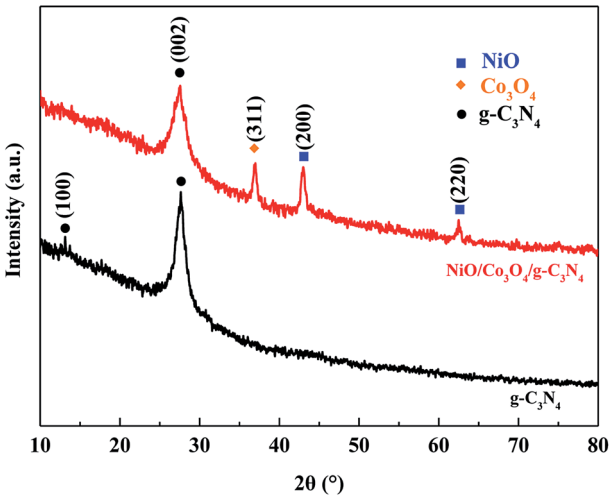

Fig. 2 XRD patterns of NiO/Co_3O_4/g-C_3N_4 and g-C_3N_4.

confirming that the layer-structured g-C_3N_4 was successfully synthesized. By comparing the XRD patterns of NiO/Co_3O_4/g-C_3N_4 nanocomposites and g-C_3N_4 sheets, it was found that the intensity of the (002) peak at 27.4° significantly decreases and the (100) peak at 13.1° disappears (Fig. 2), indicating a much-lowered long-range order in the atomic arrangements of g-C_3N_4 in the NiO/Co_3O_4/g-C_3N_4 nanocomposites. This result could be attributed to the decreased planar size and structural defects.[26,27] We also observed three new peaks at 36.8°, 43.2° and 62.9°, where the former is corresponding to the (311) plane of the cubic phase of Co_3O_4 (JCPDS no. 43-1003), and the later two peaks are both the characteristic peaks for the cubic phase of NiO (JCPDS 47-1049). These results confirmed that we have successfully prepared the NiO/Co_3O_4/g-C_3N_4 hybrid nanocomposites, in accord with the result of the HR-TEM.

The optical absorption property of the materials can considerably determine their photocatalytic activity. The UV-vis diffuse reflectance spectra (DRS) analyses of NiO/Co_3O_4/g-C_3N_4, Co_3O_4/g-C_3N_4, NiO/g-C_3N_4 nanocomposites and pure g-C_3N_4 sheets are shown in Fig. 3a. The main absorption edge of g-C_3N_4 occurred at 457 nm ($E_g = 2.71$ eV), and the NiO/g-C_3N_4, Co_3O_4/g-

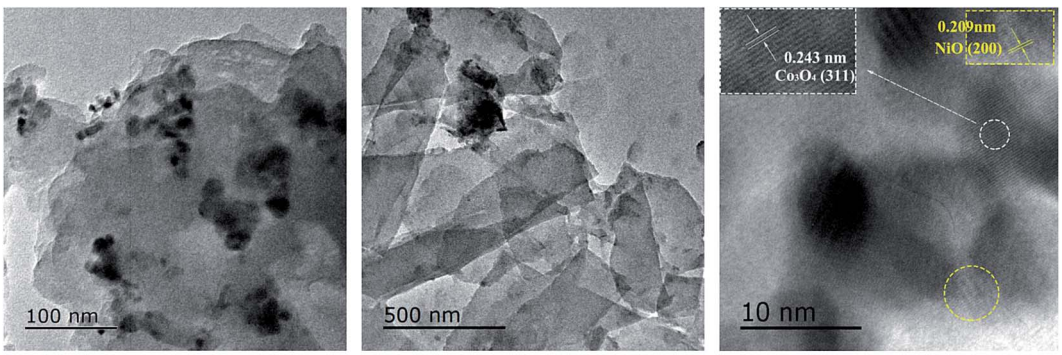

Fig. 1 TEM images of (a) NiO/Co_3O_4/g-C_3N_4 and (b) g-C_3N_4, (c) HR-TEM image of NiO and Co_3O_4 from the areas labeled by the rounded frame.

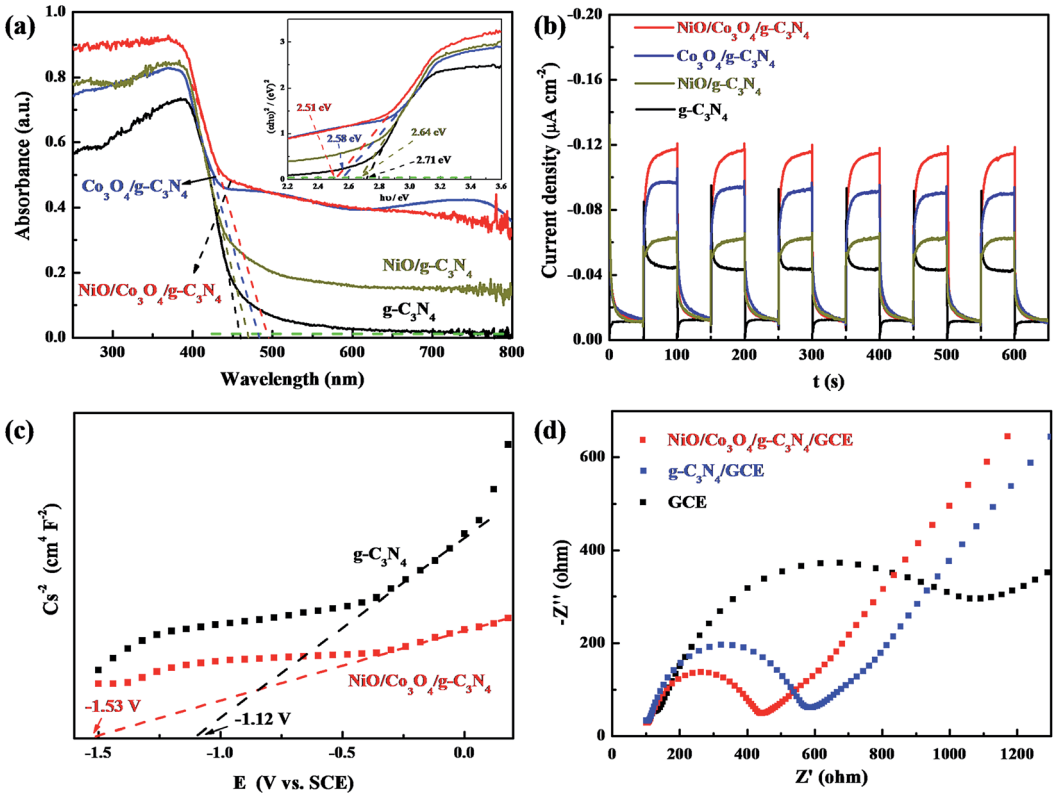

Fig. 3 (a) DRS and (b) photocurrent density *versus* time (in 0.1 mmol L^{-1} Na_2SO_4 solution) of g-C_3N_4, Co_3O_4/g-C_3N_4, NiO/g-C_3N_4 and NiO/Co_3O_4/g-C_3N_4, (c) Mott–Schottky plots of g-C_3N_4 and NiO/Co_3O_4/g-C_3N_4, (d) EIS of different electrodes in 5 mmol L^{-1} $K_3[Fe(CN)_6]$/$K_4[Fe(CN)_6]$, respectively.

C_3N_4, NiO/Co_3O_4/g-C_3N_4 nanocomposites are around 470 nm (E_g = 2.64 eV), 481 nm (E_g = 2.58 eV), 494 nm (E_g = 2.51 eV), respectively. This result indicated that NiO-doped and Co_3O_4-doped both widened the main absorption edge of g-C_3N_4 and the NiO/Co_3O_4 co-doped products exhibited the smallest band-gap, improving its conductivity. This result also implied that there was a synergistic effect between NiO and Co_3O_4 within the NiO/Co_3O_4/g-C_3N_4 nanocomposites. Interestingly, there is an extended visible-light absorption over 500–800 nm for all doped nanocomposites, which enables the possible utilization of low-energy visible light, or contributes to the high light-harvesting efficiency of the NiO/Co_3O_4/g-C_3N_4 nanocomposites.

To further investigate the photoelectric response behavior of the NiO/Co_3O_4/g-C_3N_4 nanocomposites and to understand the role of NiO/Co_3O_4 in the nanocomposites, the transient photocurrents responses were recorded in 0.1 mol L^{-1} Na_2SO_4 with repeated light on/off cycles under a 300 W xenon lamp (λ > 420 nm) irradiation (Fig. 3b). NiO/g-C_3N_4, Co_3O_4/g-C_3N_4 and NiO/Co_3O_4/g-C_3N_4 nanocomposites all show higher photocurrent densities than that of the g-C_3N_4, suggesting that NiO- or Co_3O_4-doped can improve the conductivity of g-C_3N_4. Moreover, the NiO/Co_3O_4/g-C_3N_4 nanocomposites displayed a highest photocurrent density among all samples, which indicated that there was a synergistic effect between NiO and Co_3O_4 within the NiO/Co_3O_4/g-C_3N_4 nanocomposites, in concordance with the DRS results (Fig. 3a). These results also indicated that the dramatically increased photocurrent in NiO/Co_3O_4/g-C_3N_4 nanocomposites stems from effective charge carrier separation within the nanocomposites *via* electron transfer.

Additionally, for n-type semiconductor-electrode, the donor density was calculated by the standard formula:[28]

$$\frac{1}{C^2} = \left(\frac{1}{eN_d\varepsilon\varepsilon_0}\right)|V - V_{fb}|$$

where N_d is the donor density (cm^{-3}), ε_0 is the permittivity of free space, V_{fb} is the flat-band potential (V), V is the applied potential (V), ε is the dielectric constant, and e is the electronic charge unit. Meanwhile, Fig. 3c shows the Mott–Schottky plots, typical reversed sigmoid plots of n-type semiconductors, $1/C^2$ *versus* E, for NiO/Co_3O_4/g-C_3N_4 nanocomposites and g-C_3N_4. The V_{fb} of NiO/Co_3O_4/g-C_3N_4 nanocomposites and g-C_3N_4 were estimated to be −1.53 V and −1.12 V from the Mott–Schottky results. Therefore, the N_d of NiO/Co_3O_4/g-C_3N_4 nanocomposites and g-C_3N_4 could be determined from the slope of the linear region (2.43×10^{28} cm^{-3} and 3.25×10^{27} cm^{-3}). The N_d of the NiO/Co_3O_4/g-C_3N_4 nanocomposites is 7.5-fold that of g-C_3N_4, indicating the NiO/Co_3O_4/g-C_3N_4 nanocomposites possess an improved conductivity. This result also indicated that in comparison with g-C_3N_4, the electrons could be rapidly transferred at the interface of the NiO/Co_3O_4/g-C_3N_4 nanocomposites and electrolyte, which can increase the electrochemical activity of NiO/Co_3O_4/g-C_3N_4 nanocomposites.

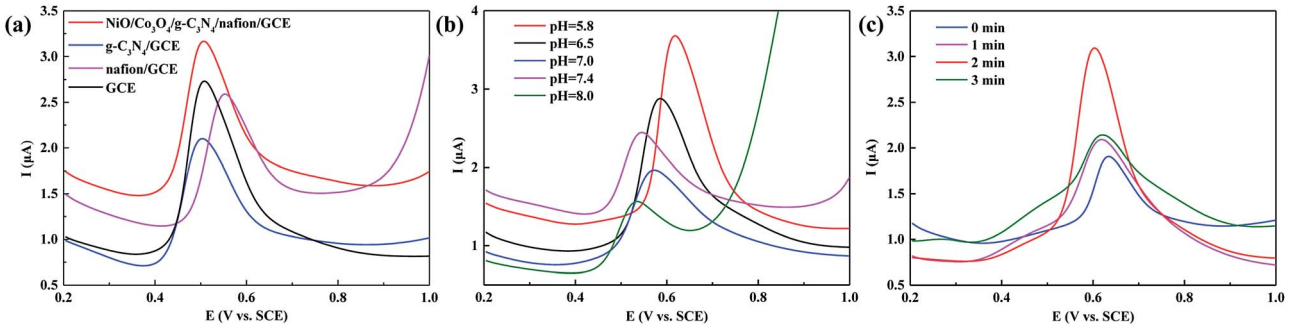

Fig. 4 Differential pulse voltammograms of (a) different modified electrodes in pH = 7.0 PBS solution; (b) different pH solutions and (c) different lighting times (0.1 mmol L^{-1} TBBP-A, scan rate: 100 mV s^{-1}).

The electrochemical impedance value is one of the most important electrochemical parameters to understand the electrode materials. Thus, the electrochemical impedance spectroscopy (EIS) was used to characterize the interfacial properties of the nanocomposites in a solution of 0.1 mol L^{-1} KCl containing 5 mmol L^{-1} $K_3[Fe(CN)_6]/K_4[Fe(CN)_6]$. The Nyquist plot of the impedance spectra of different modified electrodes are shown in Fig. 3d. Compared with g-C_3N_4/GCE and GCE, the smallest semicircles of NiO/Co_3O_4/g-C_3N_4/GCE were observed in the higher frequency region, indicating that NiO/Co_3O_4/g-C_3N_4/GCE had a lowest transfer resistance.

Moreover, we have also explored the photoelectrochemical responses of TBBP-A at the NiO/Co_3O_4/g-C_3N_4/GCE. First, the electrochemical behaviors of TBBP-A at the different modified electrodes were investigated using differential pulse voltammetry (DPV) method in pH = 7.0 phosphate buffered saline (PBS) solution (Fig. 4a). By comparing the oxidation peak current at different modified electrodes, the strongest oxidation peak current of TBBP-A is observed at NiO/Co_3O_4/g-C_3N_4/Nafion/GCE, suggesting the NiO/Co_3O_4/g-C_3N_4 nanocomposites possess the strongest photoelectrochemical activity. Then we optimized the pH of the buffer solution. Because NiO has tendency to hydrolyze at pH values <5 or above 8, we investigated pH 5.8 to 8.0 PBS solutions. The oxidation peak current of TBBP-A at NiO/Co_3O_4/g-C_3N_4/GCE was the highest in pH = 5.8 PBS solution (Fig. 4b). Hence, pH = 5.8 PBS solution was selected as buffer solution in later experiments. Furthermore, based on the success of the NiO/Co_3O_4/g-C_3N_4 nanocomposites showing improved photoelectron activity, the electrochemical sensing method for analyzing TBBP-A in water samples was performed under visible-light irradiation as a function of the irradiation time. After two minutes of light irradiation, the oxidation peak current of TBBP-A was 2.5-fold than that of no light irradiation (Fig. 4c). The reason of improved photoelectron activity can be ascribed mainly to the effective separation of electron–hole pairs within NiO/Co_3O_4/g-C_3N_4 nanocomposites under visible-light irradiation.

In addition, the relationship between peak current and scan rate is powerful tool to better understand the electrochemical performance of TBBP-A at NiO/Co_3O_4/g-C_3N_4/GCE. Thus, cyclic voltammograms (CV) at different scan rates were obtained. As shown in Fig. 5a, the relationship of the anodic (I_{pa}) peak currents *versus* the scan rate in the range 20 to 120 mV s^{-1}, whose equation is I_{pa} (μA) = 0.0219v (V s^{-1}) + 1.4533 (R = 0.995), suggesting that a controllable adsorption process occurring at NiO/Co_3O_4/g-C_3N_4/GCE.

Fig. 5b shows the DPVs of a series of different concentrations TBBP-A in pH 5.8 PBS at the NiO/Co_3O_4/g-C_3N_4/GCE. The peak current displays a gradual increase with the increasing concentration of TBBP-A. Meanwhile, the anodic peak current increases linearly with the concentrations of TBBP-A from 0.3 to

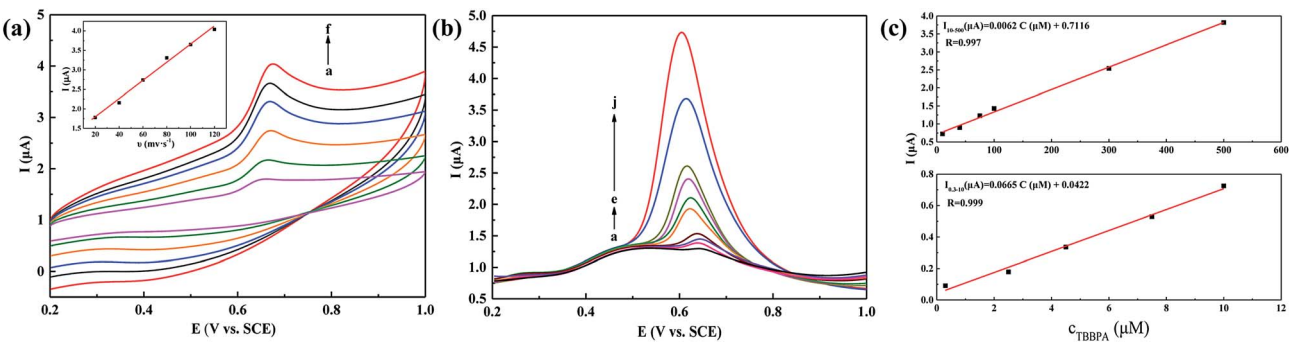

Fig. 5 (a) Cyclic voltammograms of NiO/Co_3O_4/g-C_3N_4/GCE in 0.1 mmol L^{-1} TBBP-A in pH = 5.8 PBS solution at different scan rates (from (a to f): 20, 40, 60, 80, 100 and 120 mV s^{-1}) (Inset) dependence of peak currents *vs.* scan rate. (b) Differential pulse voltammograms of NiO/Co_3O_4/g-C_3N_4/GCE in pH = 5.8 PBS containing different concentrations of TBBP-A from (a to e): 0.3 to 10 μmol L^{-1} and (e to j): 10 to 500 μmol L^{-1}; (c) calibration plot of current *vs.* concentration (0.3 to 10 μmol L^{-1} and 10 to 500 μmol L^{-1}).

Table 1 Recoveries of TBBP-A in real water samples

Sensor	Samples	No	Added	Test	RSD (%)	Recovery (%)
$NiO/Co_3O_4/g\text{-}C_3N_4/GCE$	Campus Lake water (mol L^{-1})	1	2.50×10^{-6}	2.60×10^{-6}	1.94	104.0
		2	8.00×10^{-6}	7.80×10^{-6}	0.51	97.5
		3	2.00×10^{-6}	1.88×10^{-5}	0.26	94.1
	Yangtze River water (mol L^{-1})	1	1.50×10^{-6}	1.64×10^{-6}	0.45	109.6
		2	1.80×10^{-5}	1.72×10^{-5}	1.49	95.8
		3	2.00×10^{-5}	1.89×10^{-5}	1.39	96.8

10 μmol L^{-1} and 10 to 500 μmol L^{-1} (Fig. 5c), which correspond to two liner regression equations: I_{pa} (μA) = 0.0665C (μmol L^{-1}) + 0.0422 (R = 0.999) and I_{pa} (μA) = 0.0062C (μmol L^{-1}) + 0.7116 (R = 0.999), respectively. The limit of detection is about 0.1 μmol L^{-1} (S/N = 3). But when the concentration of TBBP-A is more than 500 μmol L^{-1}, the electrochemical response becomes low, which could be attributed to the saturation of the electrode surface active sites.

Furthermore, we have investigated the electrochemical sensoring performance of the $NiO/Co_3O_4/g\text{-}C_3N_4/GCE$ in the detection of TBBP-A in real water samples. Two kind of water sample are collected from Campus Lake and Yangtze River with random sampling. As shown in Table 1, the recoveries of TBBP-A in real samples were acceptable recoveries (94.1–109.6%), suggesting that the $NiO/Co_3O_4/g\text{-}C_3N_4/GCE$ sensor could be used for detection of TBBP-A in practical water samples.

Meanwhile, the reproducibility of the modified electrode was also investigated by repetitively detecting 0.1 mmol L^{-1} TBBP-A for four times. The relative standard deviation (RSD) was 4.9%, demonstrating good reproducibility. The modified electrode was kept in refrigerator at 4 °C. After four weeks, it retained 92% of the initial peak current response, indicating that $NiO/Co_3O_4/g\text{-}C_3N_4$ film have long-term stability. The interferences were investigated in 0.1 mmol L^{-1} TBBP-A solution in the presence of bisphenol A, *o*-nitrophenol, *m*-nitrophenol, K^+, CH_3COO^- and NO_3^-, respectively (Table 2). There was no influence on the peak current, suggesting the high selectivity of the $NiO/Co_3O_4/g\text{-}C_3N_4$/Nafion/GCE for the detection of TBBP-A.

In conclusion, the functional $NiO/Co_3O_4/g\text{-}C_3N_4$ nanocomposites were synthesized by a simple method. Compared to $g\text{-}C_3N_4$, the nanocomposite reflects faster electronic conduction ability and stronger photoelectrochemical activity. An effective and sensitive detection method of TBBP-A was constructed with $NiO/Co_3O_4/g\text{-}C_3N_4/GCE$ under visible light irradiation. It displayed two linear ranges from 0.3 to 10 μmol L^{-1} and 10 to 500 μmol L^{-1} with a limit of detection of about 0.1 μmol L^{-1}. The $NiO/Co_3O_4/g\text{-}C_3N_4$ nanocomposites could be promising for applications in the field of photoelectrochemical sensing.

Table 2 Effects of the interference on the detection of 0.1 mmol L^{-1} TBBP-A

Interferences	C (mmol L^{-1})	Signal change (%)
Bisphenol A	0.003	+1.6
o-Nitrophenol	0.003	+4.9
m-Nitrophenol	0.003	+10.4
K^+	0.3	+5.7
CH_3COO^-	0.3	−0.4
NO_3^-	0.3	−7.3

Fabrication of the modified electrode

$NiO/Co_3O_4/g\text{-}C_3N_4/GCE$ was fabricated as follows: $NiO/Co_3O_4/g\text{-}C_3N_4$ nanocomposites suspension was prepared with 4.0 mg $NiO/Co_3O_4/g\text{-}C_3N_4$ dispersed into 4.0 mL of 0.1% Nafion solution. The solution was then sonicated *ca.* 10 minutes. Hereafter, bare GCE was mechanically polished to a mirror finish with 0.05 μm alumina slurry. Last, the above nanocomposites suspension of 5.0 μL was dropped on the surface of bare GCE. The modified electrode was dried naturally.

Characterization

The X-ray powder diffraction (XRD) pattern was determined on an AXS D8 Advance X-ray Diffractometer (Bruker, Germany) equipped with Cu Kα radiation (λ = 1.54 Å) source in the 2θ range from 10 to 80° at a scanning rate of 0.025° s^{-1}. The morphologies, structure and particle size of the as-prepared samples were carried out on a JSM-2100 transmission electron microscopy (TEM) (Electronics Co., Japan). The UV-vis diffuse reflectance spectra (DRS) were detected on a Cary Win 50 (Agilent, USA). The photoelectrochemical measurement was performed under a 300 W Xe lamp (Beijing Perfect Co., Ltd.). All electrochemical experiments and photoelectrochemical measurement were performed using a CHI 660E electrochemical workstation (Shanghai Chenhua Instrument Co., Ltd.) at room temperature. A three-electrode system equipped with a bare GCE or a prepared modified electrode as the working electrode, a Pt wire as the counter electrode and a saturated calomel electrode (SCE) as the reference electrode, was used for all electrochemical measurements.

Acknowledgements

This work was financially supported by National Natural Science Foundation of China (Grant. 21471122), Graduate Student Education Innovation Foundation (Grants. CX2015147 and CX2016171), and President Foundation of Wuhan Institute of Technology (Grant. 2016062).

Notes and references

1 M. Hoffmann, E. Fiedor and A. Ptak, *Toxicol. Lett.*, 2017, **269**, 15–22.
2 F. Peng, G. Ying, B. Yang, Y. Liu, H. Lai, G. Zhou, J. Chen and J. Zhao, *Environ. Toxicol. Chem.*, 2014, **33**, 1705–1711.
3 T. Debenest, A.-N. Petit, F. Gagné, M. Kohli, N. Nguyen and C. Blaise, *Chemosphere*, 2011, **85**, 50–55.
4 M. A.-E. Abdallah, S. Harrad and A. Covaci, *Environ. Sci. Technol.*, 2008, **42**, 6855–6861.
5 S. Harrad and M. A.-E. Abdallah, *Chemosphere*, 2011, **82**, 1240–1245.
6 J. Eriksson, S. Rahm, N. Green, Å. Bergman and E. Jakobsson, *Chemosphere*, 2004, **54**, 117–126.
7 Z. Zhang, A. Hibberd and J. Zhou, *Anal. Chim. Acta*, 2006, **577**, 52–61.
8 E. Blanco, M. C. Casais, M. C. Mejuto and R. Cela, *Anal. Chem.*, 2006, **78**, 2772–2778.
9 S. Chu, G. D. Haffner and R. J. Letcher, *J. Chromatogr. A*, 2005, **1097**, 25–32.
10 U. Berger, D. Herzke and T. M. Sandanger, *Anal. Chem.*, 2004, **76**, 441–452.
11 T. Hayama, H. Yoshida, S. Onimaru, S. Yonekura, H. Kuroki, K. Todoroki, H. Nohta and M. Yamaguchi, *J. Chromatogr. B: Anal. Technol. Biomed. Life Sci.*, 2004, **809**, 131–136.
12 C. Yu and B. Hu, *J. Chromatogr. A*, 2007, **1160**, 71–80.
13 J. Jin, H. Peng, Y. Wang, R. Yang and J. Cui, *Organohalogen Compd.*, 2006, **68**, 85–88.
14 R. Saint-Louis and E. Pelletier, *Analyst*, 2004, **129**, 724–730.
15 A. Covaci, S. Voorspoels, L. Ramos, H. Neels and R. Blust, *J. Chromatogr. A*, 2007, **1153**, 145–171.
16 P. Korytár, A. Covaci, P. Leonards, J. De Boer and U. T. Brinkman, *J. Chromatogr. A*, 2005, **1100**, 200–207.
17 Y. Zheng, Y. Jiao, Y. Zhu, Q. Cai, A. Vasileff, L. Li, Y. Han, Y. Chen and S. Qiao, *J. Am. Chem. Soc.*, 2017, **139**, 3336–3339.
18 J. Jiang, *RSC Adv.*, 2016, **6**, 47368–47372.
19 S. Samanta, S. Khilari, D. Pradhan and R. Srivastava, *ACS Sustainable Chem. Eng.*, 2017, **5**, 2562–2577.
20 J. Jiang, J. Zou, A. T. S. Wee and W. Zhang, *Sci. Rep.*, 2016, **6**, 34599.
21 Z. Cai, M. Rong, T. Zhao, L. Zhao, Y. Wang and X. Chen, *J. Electroanal. Chem.*, 2015, **759**, 32–37.
22 W. Gong, J. Zou, S. Zhang, X. Zhou and J. Jiang, *Electroanalysis*, 2016, **28**, 227–234.
23 J. Zhuang, W. Lai, M. Xu, Q. Zhou and D. Tang, *ACS Appl. Mater. Interfaces*, 2015, **7**, 8330–8338.
24 Y. Hou, Z. Wen, S. Cui, X. Guo and J. Chen, *Adv. Mater.*, 2013, **25**, 6291–6297.
25 F. Qi, Y. Li, Y. Wang, Y. Wang, S. Liu and X. Zhao, *RSC Adv.*, 2016, **6**, 81378–81385.
26 F. Zhao, H. Cheng, Y. Hu, L. Song, Z. Zhang, L. Jiang and L. Qu, *Sci. Rep.*, 2014, **4**, 5882.
27 Z. Zhou, Y. Shen, Y. Li, A. Liu, S. Liu and Y. Zhang, *ACS Nano*, 2015, **9**, 12480–12487.
28 K. Gelderman, L. Lee and S. W. Donne, *J. Chem. Educ.*, 2007, **84**, 685.